REACTIVE TRANSPORT: EXPERIMENTS AND PORE-NETWORK MODELLING

L. Algive, S. Bekri, M. Robin, O. Vizika
Institut Français du Pétrole, 1 et 4 avenue de Bois-Préau, 92852 Rueil-Malmaison, France

This paper was prepared for presentation at the International Symposium of the Society of Core Analysts held in Calgary, Canada, 10-12 September 2007

ABSTRACT

Dissolution and deposition phenomena are key issues in the CO_2 geological storage. In the past few years, it has been proven that CO_2 injection can lead to important pore structure modifications which mainly depend on the thermodynamic conditions, the rock and fluid composition and the flow regime. Predicting these modifications and their impact on the reservoir permeability and porosity is crucial for the success of CO_2 sequestration projects.

This paper presents an experimental and numerical study to evaluate in a comprehensive manner the impact of the deposition regimes on the relationships between permeability and porosity. Experiments have been performed in glass micromodels to visualize deposition mechanisms for different regimes. A reactive transport model using the pore-network approach has been developed to simulate the deposition phenomenon in the case of a single-phase flow. This numerical model is based on solving the macroscopic convection-diffusion equation. Its macroscopic coefficients, mean velocity, dispersion coefficient and apparent reaction term, are obtained for each unit cell of the pore network by solving analytically a set of equations describing the reactive transport at microscopic scale. The regimes that govern the deposition phenomena are numerically investigated. It is demonstrated that deposition patterns depend on both scales of the reactive transport, microscopic and macroscopic, each one being characterized by relevant dimensionless numbers.

INTRODUCTION

The CO_2 geological storage is considered as a solution to reduce its concentration in the atmosphere. Due to the high solubility of CO_2 in water and the consequent formation of acid solutions, CO_2 injection may cause dissolution of limestone and generate calcium and carbonate ions. These species may re-precipitate, because of the thermodynamic fluctuations inside the reservoir, leading to a decrease of the well injectivity. Reactive transport models have been evolved for the quantification of such phenomena.

Reactive transport, specifically acid dissolution, have been investigated by a large number of researchers. In a pioneering work, Schechter and Gidley (1969) developed an analytical approach to estimate the effects of surface reactions on petrophysical properties. A porous medium was constructed by geometrically similar cylinders,

randomly distributed, with different cross-sectional areas. Although they have taken into account only the diffusion limited process, it was shown that the largest pores would determine dissolution figures because of the higher acid concentration in these pores. Since no flow calculations were needed and no connectivity effects were considered, the influence of the hydrodynamic regime was not highlighted. More recently, reactive transport was solved either at the Darcy scale assuming a continuous porous medium (Zhang and Seaton (1994)) or at the microscopic scale in Pore Network Models. In this last case, deposition/dissolution modes were often presupposed and reaction locations were arbitrarily chosen to fit experimental data (Bhat (1998), Egermann et al. (2005)). Besides, when a global modelisation is considered, the source term of the reactive convection-dispersion equation is generally taken proportional to the mean concentration of the pore only (Christman and Edgar (1983), Rieckmann and Keil (1997)). This approach disregards the diffusion phenomenon by assuming that its characteristic time is much lower than the reaction time, so that the pore diameter does not play any role. The hypothesis seems satisfactory in the case of gaseous species but not for liquids. In the present work, diffusion mechanism is taken into account in the apparent reactivity coefficient through the set of local equations, so that the mass-transport limited phenomena can be studied.

From an experimental point of view, calcite precipitation has already been studied in "open systems" to evaluate kinetic constants (Reddy and Nancollas (1971), Shiraki and Brantley (1995), Lebron and Suarez (1996), Euvrard et al. (2004)). Lee et al. (1996) were interested in deposition in veins and determined conditions to obtain a uniform deposition. Precipitation in a 2D porous medium was not thoroughly investigated. However Dawe and Zhang (1997) observed calcium carbonate nucleation at liquid-gas interfaces in glass micromodels. Nevertheless, they did not study the deposition phenomenon, which consists of solute diffusion coupled with surface reaction.

The present paper is organized as follows. The first section describes the experimental conditions and the first experimental results. The second part is dedicated to the description of the reactive pore network model and of the results that are discussed in terms of the governing regimes. Finally, conclusions are drawn on the future works to be conducted.

EXPERIMENTS

Precipitation Mechanisms: State of the Art

Through this chapter, the choice of the experimental conditions is explained.

Calcium Carbonate Precipitation

Different chemical reactions, depending on pH, can result in calcite precipitation. For a pH value lower than the logarithm of the acid dissociation constant (pKa) of HCO_3^-, equal to 10.3 at 25°C, the main precipitation reaction is the following:

$$Ca^{2+} + 2HCO_3^- \leftrightarrow CaCO_3 + H_2O + CO_2 \quad (1)$$

When pH is higher than 10.3, the precipitation reaction is simply the reverse of the solubilisation:

$$Ca^{2+} + CO_3^{2-} \leftrightarrow CaCO_3 \quad (2)$$

The production of carbon dioxide, which may result in the creation of a gaseous phase at ambient conditions, can complicate the experimental interpretations. For this reason, the second reaction is chosen and pH is set at 13 in all the experiments performed in this study.

Precipitation Mechanisms

Whatever the reaction, precipitation can occur according to four main mechanisms (Shiraki and Brantley (1995)): homogeneous or heterogeneous nucleation, seed growth by surface adsorption and spiral growth at dislocations. The above mechanisms start only if the available energy overcomes the energetic barriers. These energies are usually expressed in terms of saturation ratio, which is a measure of the thermodynamic disequilibrium. Indeed, Gibbs energy liberated during the reaction, ΔG, and the saturation ratio, noted S, are interrelated:

$$S = \frac{a\left(Ca^{2+}\right)a\left(CO_3^{2-}\right)}{K_s} \quad \text{and} \quad S = \exp\left(\frac{\Delta G}{RT}\right) \quad (3)$$

where $a(i)$ is the activity of ion i, K_s is the solubility product of calcium carbonate, T the temperature and R the perfect gas constant.

If S is greater than unity, the solution is supersaturated but may be metastable. Actually precipitation will begin only if some nuclei are present or if the supersaturation is high enough so that nucleation occurs. The critical saturation ratio has been estimated at 40 for spontaneous homogeneous nucleation (Ghizellaoui et al. (2004)) and at 2.5 for heterogeneous nucleation (Lebron and Suarez (1996)). Heterogeneous nucleation needs much less energy because it occurs in places of high free surface energy: mainly at wall asperities. It must be specified that the above values vary with temperature or concentration of some inhibitors such as magnesium or organic carbon. The distinction between calcite growth modes depends also on supersaturation. For lower supersaturations, precipitation is controlled by growth at dislocations, whereas it is governed by simultaneous adsorption of Ca^{2+} and CO_3^{2-} onto the seed surface when S is higher (Shiraki and Brantley (1995)).

Since the reactive transport model has been developed with a kinetic law valid for adsorption, it has been decided to carry out the experiments at the highest available saturation ratio without bulk nucleation occurring. Otherwise, either the experimental time is unreasonably long or the precipitation mechanism is not similar to a deposition.

As no significant bulk nucleation was noticed for a saturation ratio equal to 75, this value has been adopted instead of 40.

Kinetics

For precipitation by adsorption, the reactive flux per unit surface, φ, is proportional to the thermodynamic disequilibrium (S-1) evaluated at the wall (Shiraki and Brantley (1995) :

$$\varphi = k \cdot \left(S_{wall} - 1\right) \tag{4}$$

where k is the intrinsic rate constant. According to Shiraki and Brantley (1995), k is equal to 2.3×10^{-5} mol.m^{-2}.s^{-1}, whereas k is equal to 6.5×10^{-3} mol.m^{-2}.s^{-1} according to Lebron and Suarez (1996). These differences can be attributed to the difficulty in proposing an intrinsic rate constant, since only global kinetic constants, including both transport towards the wall and reaction, are measured experimentally (Teng et al. (2000)).

By expressing this constant in units consistent with first-order kinetics, a mean value of 8×10^{-4} m.s^{-1} at ambient temperature conditions can be derived from the linearization near equilibrium of equation (4) for equimolar solutions.

Experimental Procedure

The glass micromodel used has a length of 18.5 cm and a width of 3.5 cm. Both of its faces are etched. The 2D network is composed of different diameter cylinders oriented 45° to the main flow direction. The mean pore-throat diameter is 0.1 mm.

The glass micromodel is initially cleaned under vacuum with sulfochromic acid in order to remove organic matter which can inhibit calcite-glass adhesion or decrease calcite growth (Lebron and Suarez (1996)). As deposition cannot begin directly on glass because of repulsive interactions, the second step consists of obtaining a uniform pre-layer of calcite. In this aim, temperature elevation, to decrease calcite solubility, and evaporation have been tested. However in a closed medium, when temperature is increasing (CO_2 solubility decreases) or solution is evaporating, the creation of bubbles is responsible for the drainage of the solution. Consequently deposition cannot be uniform. It was therefore decided to investigate a third method by depositing nuclei as homogeneously as possible. Very high theoretical supersaturation is needed so that spontaneous nucleation is predominant compared to crystal growth and to obtain numerous small particles (Euvrard et al. (2004)). To get a high supersaturation, two concentrated solutions, respectively in Ca^{2+} and CO_3^{2-}, must be used. A mixture of calcium dichloride (0.1M, 50vol.%) and sodium carbonate (0.1M, 50vol.%) is injected for three minutes at very high flow rate (200 ml.h^{-1}). It must be noted that the injection time is chosen to have a tight deposition and to avoid pore-clogging by filtration. The third step consists of obtaining the mixture required to study deposition. Since its supersaturation value is set at 75, the same solutions as previously, but a hundred times less concentrated (0.001M), are prepared. Finally, the solutions are injected simultaneously by using two pumps or by gravity flow, according to the desired flow rates. The solutions get mixed just at the inlet of the

micromodel in order to prevent precipitation in tubings or containers. During the experiments, carried out at laboratory temperature (around 20°C), image acquisition can be performed thanks to a binocular microscope.

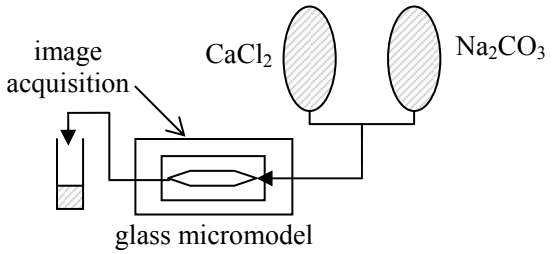

Figure 1. Schematic of experimental device.

Experimental Results

The experimental results obtained must be discussed in terms of dimensionless parameters governing the reactive transport phenomenon at local scale: Peclet-Damköhker (*PeDa*) and Peclet numbers (*Pe*). The first one compares reactive fluxes with diffusive ones while the second number is the ratio between convective and diffusive fluxes.

$$PeDa = \frac{kl}{D} \qquad Pe = \frac{vl}{D} \tag{5}$$

with l a characteristic length at the microscopic scale, D the molecular diffusion coefficient and v the mean interstitial velocity. According to earlier publications (Daccord et al. (1993), Bekri et al. (1997)), different dissolution patterns are observed depending on these numbers: a uniform dissolution for small *PeDa*, a dissolution along the main flow path for large *PeDa* and large *Pe*, and a compact dissolution at inlet or in large cavities for large *PeDa* and small *Pe*. As dissolution and deposition are similar in terms of reactive transport, this summary classification is relevant for deposition.

To check this classification, two experiments have been carried out at a fixed *PeDa* number but with two different *Pe* values. The *PeDa* number is estimated equal to 100, considering that the diffusion coefficient D is equal to 8.10^{-10} $m^2.s^{-1}$ (intermediate value between the coefficients of Ca^{2+} and CO_3^{2-}), L is equal to the mean pore-throat diameter, i.e. to 10^{-4} m, and k to 8.10^{-4} $m.s^{-1}$. Therefore, according to this *PeDa* value, the deposition pattern will depend on the flow rate. In the first experiment, the injection rate is imposed at a value of 20 $ml.h^{-1}$, which corresponds to a mean velocity of 2 $cm.s^{-1}$ and a Peclet number of about 2000. One can see on Figure 2 that deposition mainly occurs in flow paths, created by some pore clogging during nuclei deposition. Some of these calcite clusters are visible at the right of picture (b). In the pathway, the deposition layers are of the same thickness in the inlet and outlet zones of the micromodel, which confirms that convection flux is high enough to homogenise the solute concentration in the flow direction. Furthermore, the deposit seems thicker in channels than in pores, which reveals a potential role of the solute transport at the pore scale. The second experiment has been performed at a *Pe* value decreased to 10. The time optimization of the solute renewal

required not to work with a smaller Peclet number. Despite this intermediate value, the flow regime is different enough to generate another deposition pattern, which looks more like a compact deposition. One can see actually on Figure 3 that deposition is visible primarily in inlet zone (3.a). Deposition occurs in a limited area, where the concentration is high, due to rapid solute consumption with respect to convection characteristic time.

The experiments are globally explained by the classification cited above, but some divergences lie in the transition values between the regimes. For instance, it appears that the local Peclet number does not clearly govern the deposition pattern. In fact, this classification is employed for the description of the reactive transport at the pore scale. In our experiments, which are interpreted at the upper scale, the macroscopic contribution must be taken into account. This macroscopic effect will be detailed in the next part.

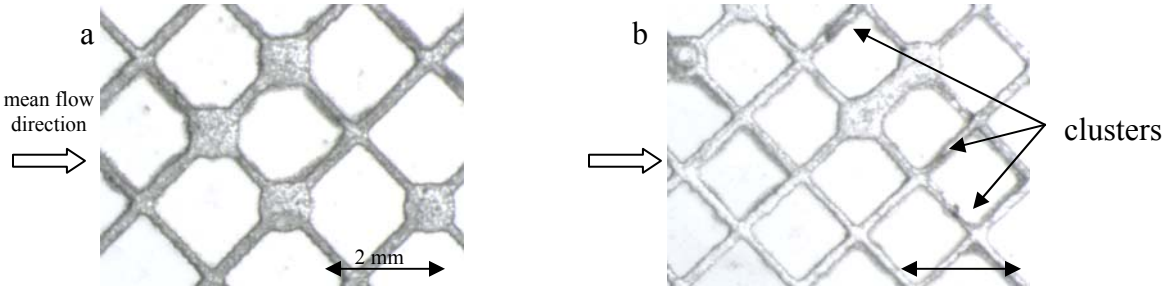

Figure 2. Pictures of calcite deposition for high *PeDa* and high *Pe*. Pictures (a) and (b) are from flow path area and dead zones of the micromodel, respectively.

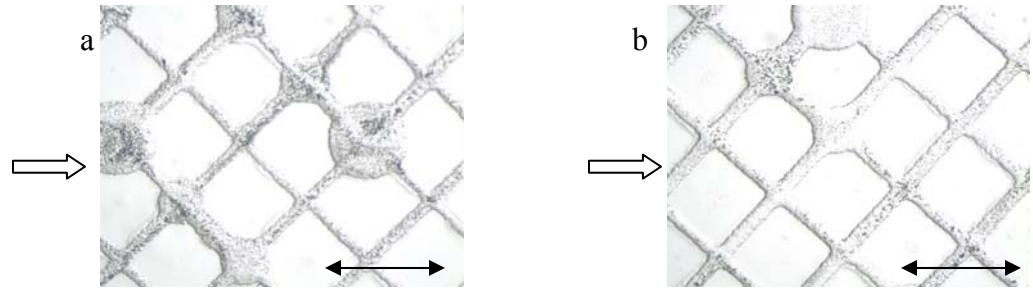

Figure 3. Pictures of calcite deposition for high *PeDa* and intermediate *Pe*. Pictures (a) and (b) are from the inlet and outlet zones of the micromodel, respectively.

REACTIVE PORE NETWORK MODEL

This section is dedicated to the modelling of the reactive-transport phenomena using the pore network approach. A reactive pore network model based on the macroscopic convection-diffusion equation has been developed to determine the evolutions of the permeability and the porosity caused by dissolution or deposition reactions. The determination of these constitutive laws (K-Φ relationships), for various governing flow and reaction regimes, is a key issue to improve the predictivity of CO_2 injection simulations.

Reactive transport

The detailed description of the pore network model (PNM) in terms of approach, model characteristics and construction can be found elsewhere (Laroche and Vizika (2005)). The network consists of a 3D cubic lattice composed of pore-bodies (nodes) interconnected by pore-throats (bonds) respecting the converging-diverging nature of the pores.

At macroscopic scale, the reactive-transport phenomenon is governed by the convection-diffusion equation below (Shapiro and Brenner (1988), Bekri et al. (1995)):

$$\frac{\partial \bar{c}}{\partial t} + \nabla \cdot \left(\bar{\mathbf{v}}^* \bar{c} - \overline{\mathbf{D}}^* \nabla \bar{c} \right) - \bar{\gamma}^* \bar{c} = 0 \tag{6}$$

where $\bar{c}$ is the average concentration in pore-bodies or pore-throats, $\bar{\mathbf{v}}^*$ the mean solute velocity vector, $\overline{\mathbf{D}}^*$ the dispersive tensor and $\bar{\gamma}^*$ the apparent reactivity coefficient.

The characteristic time of the reaction is assumed to be small compared to the time needed for the velocity field to fully develop. In other words, thermodynamic disequilibrium is considered small, so that deformation due to reaction is very slow and the no-slip condition at the wall becomes a zero-velocity condition when solving the flow equations. With this quasi-static assumption, the concentration evolution can be expressed using only the first eigenvalue of the equation (6). The other exponential functions of the linear combination are perturbations which disappear at long times, i.e. at quasi-static state. Consequently, the concentration distribution obeys to a relaxation phenomenon, whose frequency is noted Γ. Therefore, the reactive transport equation becomes:

$$-\Gamma \bar{c} + \nabla \left(\bar{\mathbf{v}}^* \bar{c} - \overline{\mathbf{D}}^* \nabla \bar{c} \right) - \bar{\gamma}^* \bar{c} = 0 \quad \text{with} \quad \bar{c} = \tilde{c} \exp\left(-\Gamma t\right) \tag{7}$$

When adimensionalizing this equation, two dimensionless numbers, Pe^* and $PeDa^*$, governing the evolution and the distribution of the macroscopic concentration $\bar{c}$, show up:

$$Pe^* = \frac{\langle \bar{v}^* \rangle L}{\langle \overline{D}^* \rangle} \qquad \text{and} \qquad PeDa^* = \frac{\langle \bar{\gamma}^* \rangle L^2}{\langle \overline{D}^* \rangle} \tag{8}$$

where L is a characteristic length at the macroscopic scale and <> is the average operator on the whole network.

Determination of the macroscopic coefficients

In order to solve the reactive convection-diffusion equation (7), the three macroscopic coefficients $\bar{\mathbf{v}}^*$, $\overline{\mathbf{D}}^*$ and $\bar{\gamma}^*$ have to be determined for each pore-throat and pore-body of the network, as for the hydraulic conductivity in the classical PNM approach. They can be defined using the three first spatial moments (Shapiro and Brenner (1988)):

$$\bar{\gamma}^* = \frac{1}{M_0}\frac{dM_0}{dt};\quad \bar{\mathbf{v}}^* = \frac{d\,\mathbf{M_1}/M_0}{dt};\quad \bar{\mathbf{D}}^* = \frac{1}{2}\frac{d}{dt}\left(\frac{\mathbf{M_2}}{M_0} - \left(\frac{\mathbf{M_1}}{M_0}\right)^2\right);\quad \mathbf{M}_i = \int c\mathbf{r}^i d^3\mathbf{r} \qquad (9)$$

where c is the local concentration and $\mathbf{r}$ is the spatial position in the pore. This local concentration and thus the three macroscopic coefficients are obtained by solving the local equations governing the reactive-transport phenomena at pore scale. The local set is composed of three equations for the local flow velocity (10), one convection-diffusion equation for the determination of the concentration profile (11), and one boundary condition at the wall taking into account a first-order surface reaction (12). The description of these equations is given in more detail in (Bekri et al. (1995)).

$$\nabla' P' = \nabla'^2 \mathbf{v}' \qquad \nabla.\mathbf{v}' = 0 \qquad \mathbf{v}'_{wall} = \mathbf{0} \qquad (10)$$

$$\nabla'^2 c' - Pe\cdot \mathbf{v}'.\nabla' c' + \frac{L^2}{D}\cdot\gamma\cdot c' = 0 \qquad (11)$$

$$\left(\nabla' c'\right)_{wall}\cdot\mathbf{n} = -PeDa\cdot c'_{wall} = -\frac{dl'}{dt'} \qquad (12)$$

According to equations (9), the apparent reactivity coefficient $\bar{\gamma}^*$ is related to the local frequency γ, which is equal to the first eigenvalue of equations (11) and (12) at quasi-static state. Consequently, $PeDa^*$ (8) and $PeDa$ are not independent, since $\bar{\gamma}^*$ is linked to this last one through γ. For the well-defined geometries used in PNM, such as capillary tubes or spheres, the local equations (10), (11) and (12) can be solved semi-analytically and $\bar{\gamma}^*$ can be given explicitly as function of $PeDa$ (Table 1). It must be noted that no empirical laws on global dissolution/deposition process are needed to estimate this coefficient. Although the attention has been focused on the apparent reactivity coefficient in this work, the same type of calculation can be used for the determination of $\bar{\mathbf{v}}^*$ and $\bar{\mathbf{D}}^*$.

Table 1. Formula of the reactive transport at the pore scale for capillaries and spheres.

	calculation $\gamma = \frac{D}{L^2}\left(\frac{\omega}{R'}\right)^2$	***concentration profile***	***deposition rate***
capillary	$\omega\cdot\frac{J_1(\omega)}{J_0(\omega)} = R'\cdot PeDa$	$\tilde{c}'(r') = \frac{\omega}{2\cdot J_1(\omega)}\cdot J_0\left(\omega\frac{r'}{R'}\right)$	$\left(\frac{\partial R'}{\partial t'}\right)_{R'} = \frac{\omega^2}{2R'}$
sphere	$1 - \frac{\omega}{\tan\omega} = R'\cdot PeDa$	$\tilde{c}'(r') = \frac{\omega^2}{3(\sin\omega - \omega\cos\omega)}\frac{\sin\left(\omega\frac{r'}{R'}\right)}{\frac{r'}{R'}}$	$\left(\frac{\partial R'}{\partial t'}\right)_{R'} = \frac{\omega^2}{3R'}$

Numerical scheme

The deposition/dissolution process is analysed as follows (Figure 4). For a given initial rock structure, the flow field is determined by solving the linear system of Poiseuille type equations using the classical pore network approach (step 1). Then, the macroscopic

convection-diffusion equation (7) can be solved (step 2) by a finite-difference scheme and a Newton-Raphson iterative process, in order to obtain the reactive fluxes and the motion of the fluid-solid interface (step 3). Then the rock structure is updated by modifying the pore-throats and pore-bodies diameters according to the deposition/dissolution fluxes (step 4). This process can be iterated (step 5) and any quantity of interest, such as permeability and porosity, can be calculated. Note that sometimes the computations cannot be done to the point of total pore clogging because of the appearance of numerical instabilities.

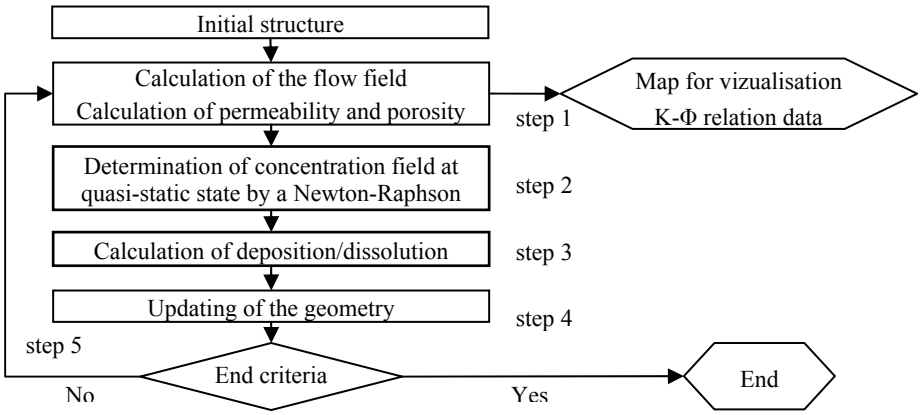

Figure 4. General scheme of the reactive transport in PNM

Numerical results and discussion

Several simulations have been performed with a periodic 10x10 2D network, in which a central main flow path, composed of large pores, has been designed (Figure 5). It appears that both scales of reactive transport, macroscopic and microscopic, must be considered to explain the deposition patterns:

- at the macroscopic scale, Pe^* and $PeDa^*$ (8) control the concentration field and thus the macroscopic chemical disequilibrium at the origin of the deposition phenomenon. More precisely, the governing number is the following ratio, which compares apparent reactive fluxes with convective and dispersive ones.

$$\beta = \frac{PeDa^*}{Pe^* + 1} \tag{13}$$

- at the microscopic scale, the deposition rate for a given macroscopic concentration is function of local *Pe* and *PeDa* (5). For the considered pore-throat and pore-bodies geometries of our model, microscopic reactive transport depends on *PeDa* only.

Thus the different dissolution/deposition regimes and their respective impacts on permeability and porosity can be classified according to β and *PeDa*.

When β is higher than one, the deposition regime is macroscopic-transport-limited, also called convection-limited by Daccord et al. (1993), who disregarded diffusion. As transport fluxes are too low to homogenize solute concentration at the network scale, $\bar{c}$ is higher in big pores. Indeed, these ones have the lowest specific area, so that the solute consumption by surface reaction seems globally less important in these volumes. Consequently, as the deposition - proportional to the chemical disequilibrium - occurs

principally in the big pores (Figure 5.a), a big porosity decrease, with respect to the permeability one, is observed (Figure 6.a).
When β is lower than one, the regime is apparent-reaction-limited. In this case, the macroscopic concentration tends to be uniform and the differences in deposit are explained by the reactive transport at the microscopic scale. If *PeDa* is smaller than unity, kinetics is surface reaction controlled so that geometry does not play any role. The deposition is therefore uniform (Figure 5.b). However, as diameters decrease relatively faster in restrictions than in pores and as permeability is function of pore-throat dimensions, the permeability decrease is more pronounced than the porosity one (Figure 6.b). For *PeDa* greater than one, i.e. if kinetics is limited by diffusion, the deposit is thicker in restrictions (Figure 5.c), for which the microscopic transport towards the wall is faster (Bekri et al. (1995)). So the permeability decrease is more accentuated than previously (Figure 6.c).
For intermediate values of β, the concentration is roughly uniform in the main flow path only. Therefore deposition cannot occur elsewhere than along this pathway, with a preference for restrictions if *PeDa* is higher than one (Figure 5.d). For dissolution, this case is close to the wormholing phenomenon described in the literature.

If comparing this classification with our experiments, one can note the exact similitude between the first test (high *Pe* and high *PeDa*) and the corresponding simulated regime (low β and high *PeDa*). β has been estimated by considering that $PeDa^*$ and Pe^* are equal to *PeDa* and *Pe* respectively. Calcite has preferentially been deposited in pore-throats, at inlet as much as at outlet, revealing the predicted uniformity of macroscopic concentration. The second experiment would correspond to the case where β and *PeDa* are high. One can observe a restricted high concentrated area, but at the micromodel inlet and not in the big pores. This confirms however that deposition pattern is explained by the concentration spatial distribution controlled by β. The modification of the main deposition location is simply linked to different boundary conditions: in the experiment, solute is renewed at the inlet, contrary to the simulation where classical periodic boundary conditions are used. In this last case, solute remains in big pores at quasi-static state, which explains the obtained deposition pattern.

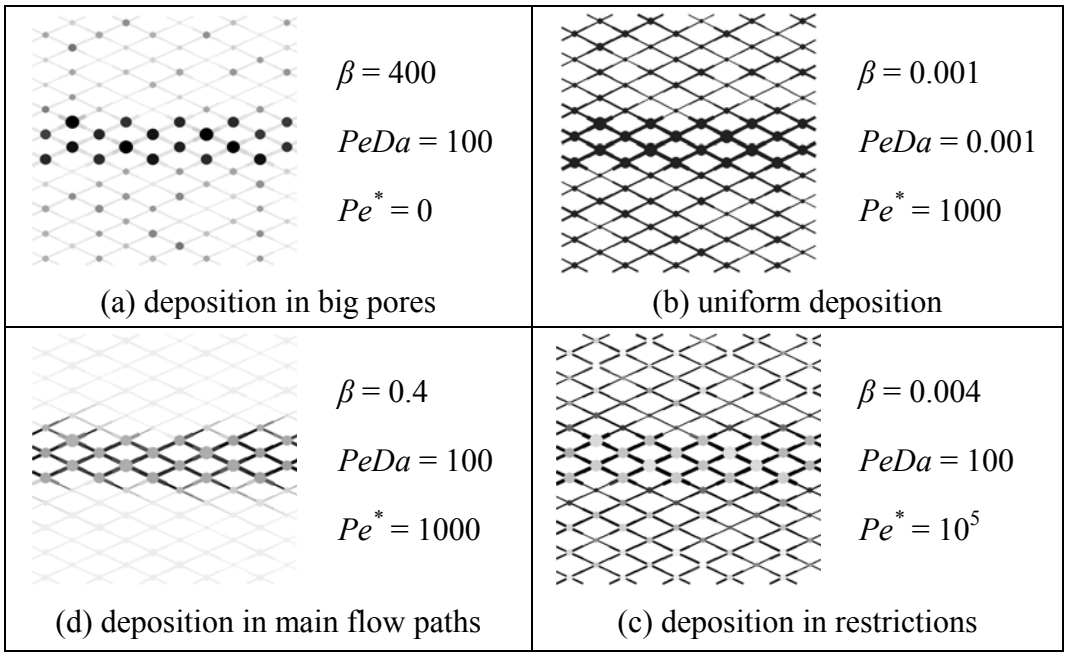

Figure 5. Deposition maps for different reactive regimes

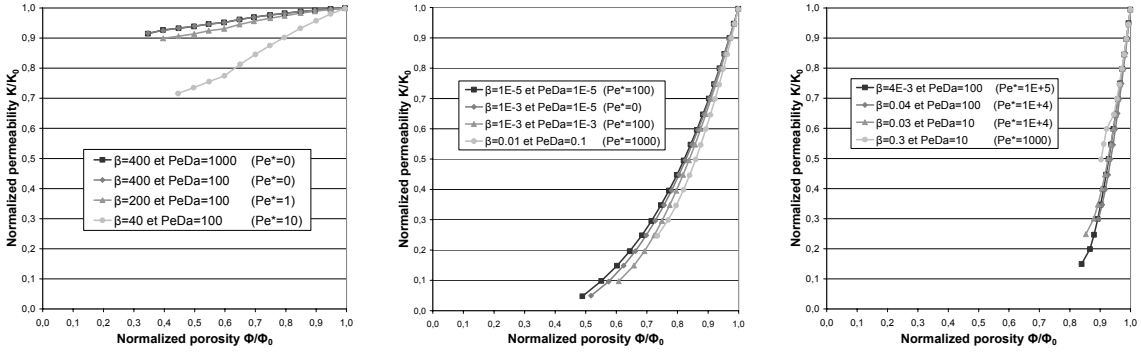

(a) deposition in pores β >>1 and *PeDa*>>1

(b) uniform deposition β <<1 and *PeDa*<<1

(c) deposition in restrictions β <<1 and *PeDa*>>1

Figure 6. Permeability versus porosity relations for different β and *PeDa*.

CONCLUSIONS

A reactive transport model using the Pore Network approach has been developed to simulate the modifications of the pore structure and the evolution of the petrophysical properties of the medium. It is based on the resolution of the reactive convection-dispersion equation at the network scale. For the basic geometries used in PNM, the apparent reactivity coefficient $\bar{\gamma}^*$ of this equation is estimated using semi-analytical relations based on the physical description of the reactive phenomenon at the pore scale. Simulations have shown that deposition patterns can only be explained by taking into

account both scales of reactive transport. At each scale, the contribution of reactive fluxes with respect to transport fluxes must be evaluated through a dimensionless number: *PeDa* at microscopic scale and $\beta=PeDa^{*}/(1+Pe^{*})$ at macroscopic scale. These numbers permit to establish a classification of the deposition regimes in agreement with the ones found in the literature. Experimentally the two deposition regimes described in the literature at high PeDa have been observed in a glass micromodel. In future works, experiments will be carried out at low PeDa. Modelling must be also extended to the two other macroscopic coefficients of the reactive equation: the mean solute velocity and the dispersive tensor. Finally other simulations should be performed on a representative network of a real porous medium in order to confirm the reactive transport classification exposed in this paper.

NOMENCLATURE

Latin Letters

$a(i)$	activity of i-species	Pe	microscopic Peclet number
c	concentration	Pe^{*}	macroscopic Peclet number
D	molecular diffusion coefficient ($m^2.s^{-1}$)	$PeDa$	microscopic Peclet-Damköhler number
D^{*}	solute dispersion tensor ($m^2.s^{-1}$)	$PeDa^{*}$	macroscopic Peclet-Damköhler number
k	intrinsic kinetic rate ($m.s^{-1}$)	R	radius (m)
K	permeability (m^2)	S	saturation ratio
K_s	solubility product	t	time (s)
L	macroscopic characteristic length (m)	$\mathbf{v}$	fluid velocity vector ($m.s^{-1}$)
l	microscopic characteristic length (m)	$\mathbf{v}^{*}$	solute velocity vector ($m.s^{-1}$)

Greek Letters

β	macroscopic reactive transport governing ratio	γ^{*}	apparent reactivity coefficient (s^{-1})
Γ	relaxation frequency at network scale (s^{-1})	Φ	porosity
γ	relaxation frequency at pore scale (s^{-1})	φ	reactive flux per unit surface ($m^2.s^{-1}$)

Subscript and superscript

$'$	dimensionless values	$\bar{}$	mean value at pore or at restriction
$_{wall}$	value evaluated at wall position	$\langle\rangle$	average operator on the whole network

REFERENCES

Bekri, S., Thovert, J.F., and Adler, P.M., "Dissolution and deposition in fractures", *Engineering Geology*, (1997), **48**, 283-308.

Bekri, S., Thovert, J.F., and Adler, P.M., "Dissolution of porous media", *Chemical Engineering Science*, (1995), **50**, 17, 2765-2791.

Bhat, S.K., "Network modeling of permeability evolution of diatomite", *SPE annual technical conference and exhibition*, New Orleans (Louisiana), (1998), 805-817.

Christman, P.G. and Edgar, T.F., "Distributed pore-size model for sulfation of limestone", *AIChE Journal*, (1983), **29**, 3, 388-395.

Daccord, G., Liétard, O., and Lenormand, R., "Chemical dissolution of a porous medium by a reactive fluid - II. Convection vs reaction, behavior diagram", *Chemical Engineering Science*, (1993), **48**, 1, 179-186.

Dawe, R.A. and Zhang, Y., "Kinetics of calcium carbonate scaling using observations from glass micromodels", *Journal of Petroleum Science and Engineering*, (1997), **18**, 3-4, 179-187.

Egermann, P., Bekri, S., and Vizika, O., "An integrated approach to assess the petrophysical properties of rocks altered by rock/fluid interactions (CO2 injection)", *SCA*, Toronto (Canada), (2005), **SCA2005-03**.

Euvrard, M., Membrey, F., Filiatre, C., and Foissy, A., "Crystallization of calcium carbonate at a solid/liquid interface examined by reflection of a laser beam", *Journal of Crystal Growth*, (2004), 265, 322-330.

Ghizellaoui, S., Lédion, J., Ghizellaoui, S., and Chibani, A., "Etude de l'inhibition du pouvoir entartrant des eaux du Hamma par précipitation contrôlée rapide et par un essai d'entartrage accéléré", *Dessalination*, (2004), **166**, 315-327.

Laroche, C. and Vizika, O., "Two-phase flow properties prediction from small-scale data using pore-network modeling", *Transport in Porous Media*, (2005), **61**, 1, 77-91.

Lebron, I. and Suarez, L., "Calcite nucleation ant precipitation kinetics as affected by dissolved organic matter", *Geochimica et Cosmochimica Acta*, (1996), **60**, 15, 2765-2776.

Lee, Y., Morse, J.W., and Wiltschko, D.V., "An experimentally verified model for calcite precipitation in veins", *Chemical Geology*, (1996), **130**, 203-215.

Reddy, M.M. and Nancollas, G.H., "The crystallization of calcium carbonate : I. Isotopic exchange and Kinetics", *Journal of Colloid and Interface Science*, (1971), **36**, 2, 166-172.

Rieckmann, C. and Keil, F.J., "Multicomponent diffusion and reaction in three-dimensional networks: General kinetics", *Industrial & Engineering Chemistry Research*, (1997), **36**, 8, 3275-3281.

Schechter, R.S. and Gidley, J.L., "The change in pore size distribution from surface reactions in porous media", *A.I.Ch.E*, (1969), **15**, 3, 339-350.

Shapiro, M. and Brenner, H., "Dispersion of a chemically reactive solute in a spatially model of a porous medium", *Chemical Engineering Science*, (1988), **43**, 551-571.

Shiraki, R. and Brantley, S.L., "Kinetics of near-equilibrium calcite precipitation at 100°C : an evaluation of elementary reaction-based and affinity-based rate laws", *Geochimica et Cosmochimica Acta*, (1995), **59**, 8, 1457-1471.

Teng, H.H., Dove, P.M., and De Yoreo, J.J., "Kinetics of calcite growth: Surface processes and relationships to macroscopic rate laws", *Geochimica et Cosmochimica Acta*, (2000), **64**, 13, 2255-2266.

Zhang, L. and Seaton, N.A., "Application of continuum equations to diffusion and reaction in pore networks", *Chemical Engineering Science*, (1994), **49**, 1, 41-50.